

**Dieses Dokument ist eine Zweitveröffentlichung (Verlagsversion) /
This is a self-archiving document (published version):**

Wolfram W. Rudolph, Gert Irmer

Hydration and ion pair formation in common aqueous La(III) salt solutions – a Raman scattering and DFT study

Erstveröffentlichung in / First published in:

Dalton Transactions. 2015, 44(1), S. 295–305 [Zugriff am: 01.11.2019]. Royal Society of Chemistry. ISSN 1477-9234.

DOI: <https://doi.org/10.1039/c4dt03003f>

Diese Version ist verfügbar / This version is available on:

<https://nbn-resolving.org/urn:nbn:de:bsz:14-qucosa2-361181>

„Dieser Beitrag ist mit Zustimmung des Rechteinhabers aufgrund einer (DFGgeförderten) Allianz- bzw. Nationallizenz frei zugänglich.“

This publication is openly accessible with the permission of the copyright owner. The permission is granted within a nationwide license, supported by the German Research Foundation (abbr. in German DFG).

www.nationallizenzen.de/



Cite this: *Dalton Trans.*, 2015, **44**, 295

Hydration and ion pair formation in common aqueous La(III) salt solutions – a Raman scattering and DFT study†

Wolfram W. Rudolph*^a and Gert Irmer^b

Raman spectra of aqueous lanthanum perchlorate, triflate (trifluorosulfonate), chloride and nitrate solutions were measured over a broad concentration (0.121–3.050 mol L⁻¹) range at room temperature (23 °C). A very weak mode at 343 cm⁻¹ with a full width at half height at 49 cm⁻¹ in the isotropic spectrum suggests that the nona-aqua La(III) ion is thermodynamically stable in dilute perchlorate solutions (~0.2 mol L⁻¹) while in concentrated perchlorate solutions outer-sphere ion pairs and contact ion pairs are formed. The La³⁺ nona-hydrate was also detected in a 1.2 mol L⁻¹ La(CF₃SO₃)₃(aq). In lanthanum chloride solutions chloro-complex formation was detected over the measured concentration range from 0.5–3.050 mol L⁻¹. The chloro-complexes in LaCl₃(aq) are fairly weak and disappear with dilution. At a concentration <0.1 mol L⁻¹ almost all complexes disappeared. In LaCl₃ solutions, with additional HCl, a series of chloro-complexes of the type [La(OH₂)_{9-n}Cl_n]⁺³⁻ⁿ (*n* = 1–3) were formed. The La(NO₃)₃(aq) spectra were compared with a spectrum of a 0.409 mol L⁻¹ NaNO₃(aq) and it was concluded that in La(NO₃)₃(aq) over the concentration range from 0.121–1.844 mol L⁻¹, nitrate-complexes, [La(OH₂)_{9-n}(NO₃)_n]⁺³⁻ⁿ (*n* = 1, 2) were formed. These nitrate-complexes are quite weak and disappear with dilution <0.01 mol L⁻¹. DFT geometry optimizations and frequency calculations are reported for a lanthanum-nona-hydrate with a polarizable dielectric continuum in order to take the solvent into account. The bond distances and angles for the cluster geometry of [La(OH₂)₉]³⁺ with the polarizable dielectric continuum are in good agreement with data from recent structural experimental measurements and high quality simulations. The DFT frequency of the La–O stretching mode at 328.2 cm⁻¹, is only slightly smaller than the experimental one.

Received 29th September 2014,
Accepted 29th October 2014

DOI: 10.1039/c4dt03003f

www.rsc.org/dalton

1. Introduction

Lanthanum is the first element of the lanthanide series and sometimes considered the first element of the period 6 transition metals. It is found in some rare-earth minerals, usually in combination with cerium and other rare earth elements. Lanthanum, a malleable, ductile, soft metal that oxidizes rapidly in air, is produced from the minerals monazite and bastnäsite using an extraction process. Lanthanum compounds have numerous applications as catalysts, additives in glass, studio lighting, laptop batteries, camera lenses and hybrid cars.¹ Lanthanum carbonate, La₂(CO₃)₃, with its generic name Fosrenol® (Shire LLC) is used as a medicine for treating renal failure.²

In aqueous solution, lanthanum exists exclusively in the trivalent state and the La³⁺ ion is strongly hydrated due to its high charge to radius ratio. Hydration numbers for La³⁺ in aqueous solution were determined using X-ray absorption fine structure (XAFS),³ X-ray diffraction (XRD),^{4–7} extended X-ray absorption fine structure (EXAFS)^{8–14} and low angle X-ray scattering (LAXS)¹² and a combined neutron scattering and X-ray scattering investigation.¹⁵ A summary of the experimental structural results obtained on aqueous La³⁺ salt solutions are presented in Table 1. The EXAFS and LAXS investigations resulted at a coordination number at 9 for the first hydration shell while XRD studies indicated 8–9 water molecules in the first sphere.^{3–6} The XRD studies were carried out on concentrated LaCl₃ and LaBr₃ solutions (1.4–3.808 mol L⁻¹) while EXAFS and XAFS studies were carried out on dilute or moderately concentrated ones. These high concentrations, however, pose a challenge because in aqueous trivalent metal ion solutions complex formation is common and therefore La³⁺(aq) may form complexes with common ions such as chloride, bromide and nitrate. The direct coordination of La³⁺ may influence the spectroscopic results and the observed spread in the

^aMedizinische Fakultät der TU Dresden, Institut für Virologie im MTZ, Fiedlerstr. 42, 01307 Dresden, Germany. E-mail: Wolfram.Rudolph@tu-dresden.de

^bTechnische Universität Bergakademie Freiberg, Institut für Theoretische Physik, Leipziger Str. 23, 09596 Freiberg, Germany

†Electronic supplementary information (ESI) available. See DOI: 10.1039/c4dt03003f

Table 1 Coordination numbers and La–O bond distances for aqueous La³⁺-salt solutions at room temperature (298/296 K)

Method	Solution composition	La ³⁺ /mol L ⁻¹	CN	La–O bond distance/Å	Remarks	Ref.
XRD	LaCl ₃	1.54–2.67 mol kg ⁻¹	8.0 ± 0.2	2.48 ± 0.01	With and without HCl; outer-sphere Cl ⁻ , La ³⁺ ...Cl ⁻ 4.7 Å	6
XRD	LaBr ₃	2.66 mol kg ⁻¹	8.0 ± 0.2	2.47	Outer-sphere Br ⁻ , La ³⁺ ...Br ⁻ 4.8 Å	7
	LaBr ₃ + HBr excess	2.95 mol kg ⁻¹	7.9 ± 0.2	2.48		
XRD	La(ClO ₄) ₃	2.88	8.0 ± 0.3	2.57 ± 0.005		5
	La ₂ (SeO ₄) ₃	0.70	8.0 ± 0.3	2.56 ± 0.005		
XRD	LaCl ₃	3.808 mol kg ⁻¹	9.13 ± 0.1	2.58 ± 0.01	Outer-sphere Br ⁻ , La ³⁺ ...Cl ⁻ 5.0 Å	4
XAFS	La(NO ₃) ₃	0.007	8.3 ± 0.1	2.59 ± 0.02	Temperature dependent measurements	3
XRD	LaCl ₃	3.17–0.46 mol kg ⁻¹	6 La–O _{prism} 3 La–O _{capp.}	2.564 ± 0.005 2.723 ± 0.01	Simulation of La K-edge EXAFS spectra (model with 8 waters has been used as well)	8
EXAFS	LaBr ₃	3.40–0.51 mol kg ⁻¹	6 La–O _{prism} 3 La–O _{capp.}	2.573 ± 0.005 2.744 ± 0.005		
EXAFS	LaCl ₃	0.05–0.20	12 ± 0.5	2.56 ± 0.01		9
EXAFS	La(ClO ₄) ₃	0.80	9	2.545 ± 0.002		10
EXAFS	LaCl ₃ /HCl	0.10 + 0.25 HCl	9.2 ± 0.37	2.54 ± 0.002	Fully hydrated La ³⁺ chloro-complex: CN(Cl ⁻) = 2.10, La–Cl = 2.92 ± 0.003 Å	11
	LaCl ₃ /LiCl	0.10 + 14 LiCl	6.5 ± 0.2 (O) 2.1 ± 0.2 (Cl)	2.57 ± 0.002 2.92 ± 0.003		
EXAFS/LAXS	La(ClO ₄) ₃	0.662	6 La–O _{prism} 3 La–O _{capp.}	2.514 ± 0.015 2.64 ± 0.02		12
EXAFS	[La(H ₂ O) ₉](CF ₃ SO ₃) ₃	0.2	6 La–O _{prism} 3 La–O _{capp.}	2.514 ± 0.007 2.64 ± 0.009		13
EXAFS	La(H ₂ O) ₉ (CF ₃ SO ₃) ₃	0.2	6 La–O _{prism} 3 La–O _{capp.}	2.549 ± 0.007 2.641 ± 0.009	K-edge data	14
ND, XRD, EXAFS	LaCl ₃	1.0 mol kg ⁻¹	8 La–O _{H₂O} 1 La–Cl	2.53 2.82		15

La–O bond distances for La³⁺(aq) in the first hydration sphere as well as the numbers for the hydration number from 8⁶ to 12⁴ waters may be an explanation. An EXAFS and LAXS structure study on La(ClO₄)₃(aq)¹² concluded that the most probable hydration structure of La³⁺ is a 9-fold coordination by water molecules forming a local geometric configuration of a tricapped trigonal prism (TTP) with D₃ symmetry. The O-atoms of the three waters in the equatorial plane (capping position) are separated from the cation by a bond distance at 2.64 Å, while six water molecules at the vertices of the trigonal prism have a La–O bond distance at 2.515 Å. In addition to the experimental work, computer simulations significantly contributed to clarifying the details of the structure and dynamics of the waters in the first hydration shell of La³⁺ (ref. 16–20) and the latest high quality studies have confirmed the La³⁺ nona-hydrate structure.

Vibrational spectroscopy, especially Raman spectroscopy, is frequently used to characterize hydrated metal ions and related species in aqueous solution. It is especially useful to characterize the species formed at the molecular level such as hydrated ions, ion pairs between metal ions and anions and hydrolysis. Raman scattering measurements on aqueous La³⁺ should allow, in principle, the characterization of the solution structure in greater detail. However, aqueous La³⁺ solutions have been measured by Raman spectroscopy only on a few occasions.^{21–23} ‡ Due to the limitations of Raman spectroscopy in the past, the spectra in the low frequency range^{21,22} were of

low quality. It has been shown on a variety of aqueous metal salt solutions that for meaningful Raman spectroscopic analysis R-normalized spectra were necessary in the terahertz frequency range^{23–27} in order to account for the Bose-Einstein correction and the scattering factor.²⁸ It seemed, therefore, warranted to extensively study aqueous lanthanum salt solutions over a large concentration range and with different counter ions.

This study was undertaken to characterize the hydration and speciation in aqueous La³⁺ solutions and to this end lanthanum(III) salt solutions of common anions were studied over a broad concentration range and down to low wavenumbers (terahertz frequency range). Triflate and perchlorate are considered non-complex-forming anions and were therefore chosen to measure the La–O stretching mode in aqueous solution in order to characterize the hydration sphere of La³⁺(aq). A La(ClO₄)₃ solution in heavy water was measured in order to characterize the vibrational isotope effect by changing from [La(H₂O)₉]³⁺ to [La(D₂O)₉]³⁺. In chloride- and nitrate-metal salt solutions, however, it was shown that these anions readily form complexes with a variety of di- and trivalent metal cations^{24–27} and the question arises as to whether these complexes also occur with La³⁺(aq). The following aqueous systems were measured by Raman spectroscopy at 23 °C: La(ClO₄)₃ and La(ClO₄)₃ plus HClO₄, La(CF₃SO₃)₃, LaCl₃ and LaCl₃ plus additional HCl and La(NO₃)₃. Specifically, we were interested in the vibrational characterization of the La³⁺-aqua stretching band as a function of solute concentration and the possible formation of ion pairs/complexes between La³⁺ and the anions.

‡ For preliminary data on aqueous La³⁺-salt solution cf. ref. 23.

To verify the spectroscopic assignment for the La–O stretching band, a lanthanum-water cluster with nine waters was modeled using density functional theory (DFT) calculations. The gas phase cluster with first shell water molecules, the nona-aqua cluster of La^{3+} , $[\text{La}(\text{OH}_2)_9]^{3+}$ and the nona-aqua clusters of La^{3+} with a polarizable dielectric continuum (PC model) were found as stable clusters. The frequency calculations were carried out on the $[\text{La}(\text{OH}_2)_9]^{3+}$, the cluster with a polarizable dielectric continuum in order to include the solvent effect.

2. Experimental details; data analysis and *ab initio* molecular La^{3+} -water cluster calculations

2.1. Preparation of solutions

Lanthanum perchlorate solutions were prepared from La_2O_3 (Sigma-Aldrich, 99.9%) and HClO_4 in a beaker until all oxide dissolved. The lanthanum ion content was analysed by complexometric titration.²⁹ The solution density was determined with a pycnometer at 23 °C and the molar ratios water per salt were calculated (R_w -values). A $\text{La}(\text{ClO}_4)_3$ stock solution was prepared at 2.488 mol L^{-1} ($R_w = 15.72$). This solution was acidic with a pH value at ~ 3 . For Raman spectroscopic measurements the solutions were filtered through a fine sintered glass frit (1–1.6 μm pore size). The solutions showed no Tyndall effect and were “optically empty” (see *e.g.* ref. 30). From this stock solution, the following dilution series was prepared: 2.165 mol L^{-1} ($R_w = 18.48$), 1.244 mol L^{-1} ($R_w = 37.24$), 0.622 mol L^{-1} ($R_w = 81.54$), 0.498 mol L^{-1} ($R_w = 103.43$) and 0.249 mol L^{-1} ($R_w = 213.75$). The solutions were analyzed for dissolved chloride with a 5% AgNO_3 solution. The absence of a white AgCl precipitate proved that the stock solution was free of Cl^- . Furthermore, two solutions with an excess of perchloric acid were prepared ($\text{La}(\text{ClO}_4)_3$ plus HClO_4): (A) 2.160 mol L^{-1} $\text{La}(\text{ClO}_4)_3$ + 1.518 mol L^{-1} $\text{HClO}_4(\text{aq})$, (B) 1.080 mol L^{-1} $\text{La}(\text{ClO}_4)_3$ + 0.759 mol L^{-1} HClO_4 .

A 1.20 mol L^{-1} $\text{La}(\text{CF}_3\text{SO}_3)_3$ solution was prepared from crystalline $\text{La}(\text{CF}_3\text{SO}_3)_3$ (Sigma-Aldrich, 99.9%) and triply distilled water.

Three LaCl_3 solutions were prepared from $\text{LaCl}_3 \cdot 6\text{H}_2\text{O}$ (Sigma, 99.9%) and triply distilled water and the lanthanum content was analysed by complexometric titration. The solution concentrations were determined at 3.050 mol L^{-1} ($R_w = 16.07$), 2.03 mol L^{-1} ($R_w = 25.20$) 1.017 mol L^{-1} ($R_w = 52.46$) and 0.051 mol L^{-1} ($R_w = 107.07$). Furthermore, two solution series with an excess of HCl were prepared (LaCl_3 plus HCl): (A) 2.03 mol L^{-1} LaCl_3 + 1.00 mol L^{-1} HCl and 2.03 mol L^{-1} LaCl_3 + 4.00 mol L^{-1} HCl and a second series 1.017 mol L^{-1} LaCl_3 + 1.00 mol L^{-1} HCl and 1.017 mol L^{-1} LaCl_3 + 4.00 mol L^{-1} HCl .

Four $\text{La}(\text{NO}_3)_3$ solution were prepared from $\text{La}(\text{NO}_3)_3 \cdot 6\text{H}_2\text{O}$ and triply distilled water: 1.844 mol L^{-1} ($R_w = 26.09$), 1.050 mol L^{-1} ($R_w = 49.10$), 0.466 mol L^{-1} ($R_w = 115.26$) and 0.121 mol

L^{-1} ($R_w = 455.3$). The $\text{La}(\text{III})$ contents and the solution densities were determined as mentioned above.

2.2. Spectroscopic measurements

Raman spectra were measured in the macro chamber of the T 64000 Raman spectrometer from Jobin Yvon in a 90° scattering geometry at 23 °C. These measurements have been already described elsewhere in detail.^{28,31} Briefly, the spectra were excited with the 514.5 nm line of an Ar^+ laser at a power level of 1100 mW at the sample. After passing the spectrometer in subtractive mode, with gratings of 1800 grooves mm^{-1} , the scattered light was detected with a cooled CCD detector. I_{VV} and I_{VH} spectra were obtained with fixed polarisation of the laser beam by rotating the polarizer at 90° between the sample and the entrance slit to give the scattering geometries:

$$I_{\text{VV}} = I(\text{Y}[\text{ZZ}]\text{X}) = 45\alpha^2 + 4\gamma^2 \quad (1)$$

$$I_{\text{VH}} = I(\text{Y}[\text{ZY}]\text{X}) = 3\gamma^2. \quad (2)$$

The isotropic spectrum, I_{iso} is then constructed:

$$I_{\text{iso}} = I_{\text{VV}} - 4/3 \cdot I_{\text{VH}}. \quad (3)$$

The depolarization ratio, ρ , of the modes was determined according to eqn (4):

$$\rho = I_{\text{VH}}/I_{\text{VV}} = 3\gamma^2/(45\alpha^2 + 4\gamma^2). \quad (4)$$

The polarization analyser was calibrated with CCl_4 before each measuring cycle and adjusted if necessary. The depolarisation ratio of the ν_1 mode at 459 cm^{-1} was determined at 0.0036 ± 0.0005 (15 independent measurements). The depolarization ratios of the depolarized CCl_4 bands at 217 cm^{-1} and 315 cm^{-1} were determined at 0.75 ± 0.02 .

In order to obtain spectra defined as $I(\bar{\nu})$ which are independent of the excitation wavenumber ν_L , the measured Stokes intensity should be corrected for the scattering factor $(\nu_L - \bar{\nu})^3$. In the case of counting methods used, the measured count rates were corrected with the factor $(\nu_L - \bar{\nu})^3$. The spectra were further corrected for the Bose-Einstein temperature factor, $B = [1 - \exp(-h\bar{\nu}c/kT)]$ and the frequency factor, $\bar{\nu}$, to give the so called reduced or $R_Q(\bar{\nu})$ spectrum. It is also possible to calculate the isotropic spectrum in R-format from the R_{VV} and R_{VH} spectra according to eqn (5):

$$R_Q(\bar{\nu})_{\text{iso}} = R_Q(\bar{\nu})_{\text{VV}} - 4/3 R_Q(\bar{\nu})_{\text{VH}}. \quad (5)$$

In the low wavenumber region, the $I(\bar{\nu})$ and $R_Q(\bar{\nu})$ spectra are significantly different and only the spectra in R-format are presented. It should be noted that one of the advantages of using isotropic R-spectra is that the baseline is almost flat in the 40–700 cm^{-1} wavenumber region allowing relatively unperturbed observation of any weak modes present.^{28,31,32}

Density functional theory (DFT) calculations were carried out using the Gaussian03 package³³ employing the unrestricted B3LYP functional. The B3LYP uses the semi-local correlation functional expressed in ref. 34 and a hybrid three-

parameter exchange functional devised by Becke.³⁵ For these computations the effective core potentials (ECPs) were used for La^{3+} and all-electron basis sets were used for all other atoms. Geometry optimizations for the cluster $[\text{Ln}(\text{H}_2\text{O})_9]^{3+}$ were performed without symmetry restrictions with a mixed basis set LANL2DZ (Los Alamos National Laboratory 2 Double Zeta) for La and 6-31G (double-zeta Pople type) basis set for the atoms O and H. The basis set LANL2DZ uses a relativistic ECP for the inner electrons and the D95V (Dunning/Huzinaga valence double-zeta) basis set for the 11 valence electrons. The inclusion of solvent effects on geometry and vibrational frequencies of $[\text{Ln}(\text{H}_2\text{O})_9]^{3+}$ was taken into account by placing the cluster within the solvent water. For this purpose, the Polarized Continuum Model (PCM) implemented in the GAUSSIAN package was used in a version described in ref. 36 where the solvent is modelled as an isotropic and homogeneous continuum, characterized by its dielectric properties. The cavity consists of a set of interlocking spheres attached to the solute atoms. The electrostatic solute–solution interaction is calculated introducing an apparent charge distribution spread on the cavity surface. Solvent polarization must be included to take into account the bulk water effect on the La^{3+} -water cluster and in order to achieve a good agreement with experiment.

A comparative *ab initio* Hartree–Fock (HF) and DFT investigation was also carried out in order to visualize the influence of the used methods and two different basis sets (one with polarization functions) on the bond length and the symmetric La–O stretching frequency of $[\text{La}(\text{H}_2\text{O})_9]^{3+}$. Again, $[\text{La}(\text{H}_2\text{O})_9]^{3+}$ in the gas phase and embedded in a polarizable continuum were considered (results and discussion see Table S1†).

3. Results and discussion

3.1. $[\text{La}(\text{OH}_2)_9]^{3+}(\text{aq})$

The $\text{La}^{3+}(\text{aq})$ ion is hydrated by nine water molecules and forms a tricapped trigonal prismatic coordination polyhedron (symmetry D_3) which also exists in the crystalline compound $[\text{La}(\text{H}_2\text{O})_9](\text{CF}_3\text{SO}_3)_3$.^{13,14} The oxygen atoms of the three water molecules in the equatorial plane are separated from La^{3+} by a bond distance of 2.64 Å, while the six water molecules at the

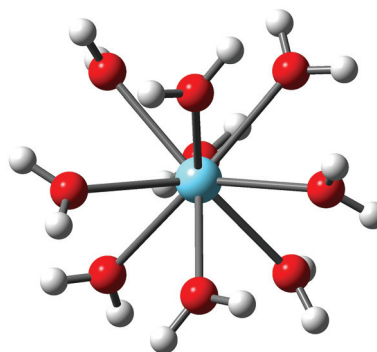


Fig. 1 Structure of the nona-aqua La^{3+} -ion (D_3 – symmetry).

vertices of the trigonal prism are found at an average distance La–O bond distance of 2.515 Å.¹² Our optimized $[\text{Ln}(\text{H}_2\text{O})_9]^{3+}$ structure resulted in a tricapped trigonal prism (TTP) geometry of symmetry D_3 (see Fig. 1) comparable to the ones found by both experimental and theoretical studies.^{12–20} The difference obtained between the three equatorial La–O distances and the six axial La–O distances is smaller than the ones found from structural experiments but the mean La–O bond distance agrees well with experimental values. Depending on the fit procedure with one or two shells applied to the experimental results one or two bond distances were obtained. Our DFT results are given in Table 2 together with the experimental data and high level simulation results. The tricapped trigonal prism (TTP) is now well established as the coordination polyhedron for La^{3+} . The hydration sphere of $\text{La}^{3+}(\text{aq})$ is labile and a water-exchange rate constant k_{ex} at 25 °C was given at ≥ 0.2 ns (estimated from $\text{H}_2\text{O}-\text{SO}_4^{2-}$ interchange rates) and a water residence time $\tau = 5$ ns follows.^{37,38} Helm and Merbach³⁹ proposed that the mechanistic path for water exchange for La^{3+} and the lighter lanthanides would follow an I_d mechanism, in which the transition state changes from nine water molecule neighbors to eight and then back to nine. This involves changing the local ion hydration geometry from a TTP to a square antiprism (SAP) and then back to the TTP. Because of the labile coordination sphere for La^{3+} there is the possibility of a counterion (anion) coordination replacing water from the coordination polyhedron.¹⁵

Table 2 Geometrical parameters such as bond distances (Å) and bond angles (°) of $[\text{Ln}(\text{H}_2\text{O})_9]^{3+}$ imbedded in a polarizable dielectric continuum. Comparison of our DFT calculations with published MD simulation and experimental results

Bond distances and angles	Our DFT results	Ref. 18 ^a	Ref. 18 ^b	Ref. 4 ^c	Ref. 12 ^d	Ref. 14 ^e	Ref. 14 ^f	Ref. 14 ^g	Ref. 14 ^h
La–O(eq)	2.576	2.58	2.52	2.580	2.64	2.618	2.596	2.549	2.542
La–O(ax)	2.560	2.52			2.515	2.525	2.515		
O(eq)–H(eq)	0.986								
H(eq)–O(eq)–H(eq)	110.2								
O(ax)–H(ax)	0.985								
O(ax)–H(ax)	110.4								

^a MD, two-shell model. ^b MD, one-shell model. ^c X-ray, one-shell model. ^d Large angle X-ray scattering, two-shell model. ^e EXAFS, two-shell model, K-edge data. ^f EXAFS, one-shell model, L_3 -edge data. ^g EXAFS, two-shell model, K-edge data. ^h EXAFS, one-shell model, L_3 -edge data.

Considering the water molecules as point masses, the LaO_9 skeleton of the nona-hydrate $[\text{La}(\text{OH}_2)_9]^{3+}$ possesses D_{3h} symmetry and with its 10 atoms, 24 normal modes (n.m.) are expected. The irreducible representation of the vibrational modes is as follows: $\Gamma_{\text{vib}}(D_{3h}) = 3a'_1(\text{Ra}) + a'_2 + 5e'(\text{Ra, i.r.}) + a''_1 + 3a''_2(\text{i.r.}) + 3e''(\text{Ra})$. Two stretching modes and a bending mode are expected with character a'_1 and these modes are Raman active only. Two stretching modes and three bending modes occur with character e' and these modes are infrared and Raman active. A stretching mode and two bending modes for character a'_2 are expected and these n.m. are infrared active only while three modes (one stretch and two bending modes) with character e'' are only Raman active. The modes with character a'_2 and a''_1 are torsional modes and are not active. However, it is unlikely that such a large number of n.m. will be observed in Raman scattering because in reality the spectra are not ideal and weak, broad bands may not be detectable in the aqueous solution state. In particular for metal ion-oxygen bands in aqueous solution only the strongest band(s) may be observed. Furthermore, the hydration sphere is flexible and an ultrafast exchange occurs between the water molecules in the first shell and the bulk.

The water molecules of the lanthanum aqua complex couple only slightly and can be viewed as point masses. The 78 n.m. expected for $[\text{La}(\text{OH}_2)_9]^{3+}$ may be divided into 27 internal and 27 external modes of the nine coordinated water molecules plus the already mentioned 24 n.m. of the LaO_9 skeleton. Generally, the water molecules in the metal-aqua complex possess weak, broad modes below 1200 cm^{-1} (see Fig. 2). The vibrations are derived from the rotational- and translation degrees of freedom of the isolated water molecule. The vibrations of these water molecules (ligands) from the $[\text{La}(\text{OH}_2)_9]^{3+}$ complex result in librational modes: wag, twist, and rock.⁴⁰ In addition to these librational modes, the internal water modes are observed, namely $\nu_2(\text{H}_2\text{O})$, the deformation mode and two stretching modes, ν_1 and ν_3 OH. The deformation mode in liquid water is found at 1640 cm^{-1} and the stretching modes at $\sim 3400 \text{ cm}^{-1}$ as a very broad structured band. The water modes are modified when coordinated to metal ions such as La^{3+} but are difficult to separate from the contributions of the librational and internal water modes of the bulk phase. The LaO_9 skeleton modes, however, should be easier to detect although they are sometimes quite weak. In liquid water, the H-bonded water molecules also show broad and weak librational modes as well as the internal water bands such as the deformation band, $\delta \text{H}_2\text{O}$, and the stretching O–H bands. A summary of the spectra of liquid water and heavy water, its bands and band assignments is given elsewhere.^{40–43}

3.2. $\text{La}(\text{ClO}_4)_3(\text{aq})$ and $\text{La}(\text{CF}_3\text{SO}_3)_3(\text{aq})$ – characterization of $[\text{La}(\text{OH}_2)_9]^{3+}$

The $\text{La}(\text{ClO}_4)_3$ solution spectra reveal a Raman mode for the $[\text{La}(\text{OH}_2)_9]^{3+}$ species, which is very weak, strongly polarized and broad positioned at $\sim 343 \text{ cm}^{-1}$. The Raman spectrum in R-format of a 2.488 mol L^{-1} $\text{La}(\text{ClO}_4)_3$ solution is presented in Fig. 2. In neither $\text{NaClO}_4(\text{aq})$ nor $\text{HClO}_4(\text{aq})$ was this mode

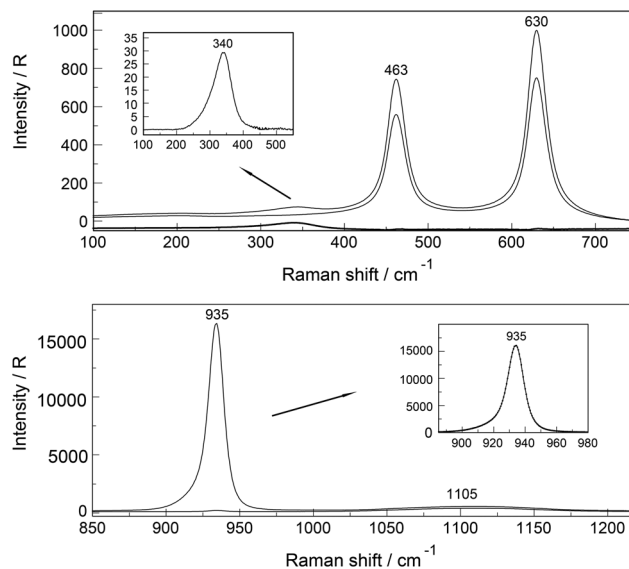


Fig. 2 Raman scattering profiles of a 2.488 mol L^{-1} ($R_w = 15.7$) $\text{La}(\text{ClO}_4)_3(\text{aq})$. Upper panel, low wavenumber region: Shown are the R_{pol} and R_{depol} scattering profiles and underneath the isotropic profile R_{iso} . Note the broad and very weak scattering contribution at 340 cm^{-1} which is strongly polarized. In addition the deformation modes of $\text{ClO}_4^-(\text{aq})$ at 463 cm^{-1} and 630 cm^{-1} are shown. The inset shows the weak isotropic band at 340 cm^{-1} in more detail. Lower panel, high wavenumber region: Shown are the R_{pol} and R_{depol} scattering profiles. The strongest $\text{ClO}_4^-(\text{aq})$ band, $\nu_1(a_1)$ at 935 cm^{-1} is presented as well as the broad much weaker deformation mode of $\text{ClO}_4^-(\text{aq})$, $\nu_3(f_2)$. The inset shows the $\text{ClO}_4^-(\text{aq})$ band, ν_1 at 935 cm^{-1} in greater detail.

observed and must therefore stem from the vibration connected to a La–O stretching band. This mode shows an asymmetry at lower wavenumber $\sim 308 \text{ cm}^{-1}$ and a slight concentration dependence of the peak position of this band was observed. In going from 2.488 mol L^{-1} to a fairly dilute La-perchlorate solution at 0.249 mol L^{-1} this mode becomes much narrower and shifts 3 cm^{-1} to higher wavenumbers at 343 cm^{-1} and the asymmetry disappears with dilution. This concentration effect with respect to peak position and fwhh of the La–O stretching mode in $\text{La}(\text{ClO}_4)_3(\text{aq})$ is given in Fig. S1 of the ESI.† The concentration profile of the $\nu_1 \text{LaO}_9$ band of three $\text{La}(\text{ClO}_4)_3$ solutions is presented in Fig. 3.

Although the perchlorate ion (see Fig. 2) was chosen as the counterion because it is known as a non-complexing anion, penetration into the first hydration sphere of the La^{3+} seems plausible in the most concentrated $\text{La}(\text{ClO}_4)_3(\text{aq})$. In the $\text{La}(\text{ClO}_4)_3(\text{aq})$ at 2.488 mol L^{-1} , the mole ratio solute to water is 15.7 and this water content is barely enough to completely hydrate the La^{3+} ion while the remaining 6.7 water molecules hydrate the three ClO_4^- ions. It becomes clear that in concentrated solutions contact ion pair formation is simply forced on La^{3+} by penetration of ClO_4^- into the first coordination shell of the cation. At such a concentration state outer-sphere ion pairs, $[\text{La}(\text{OH}_2)_9]^{3+} \cdot \text{ClO}_4^-$, must exist in equilibrium with contact ions pairs ($\text{La}^{3+} \cdot \text{ClO}_4^-$). These ion pairs may explain the slight concentration dependent shoulder at 308 cm^{-1} men-

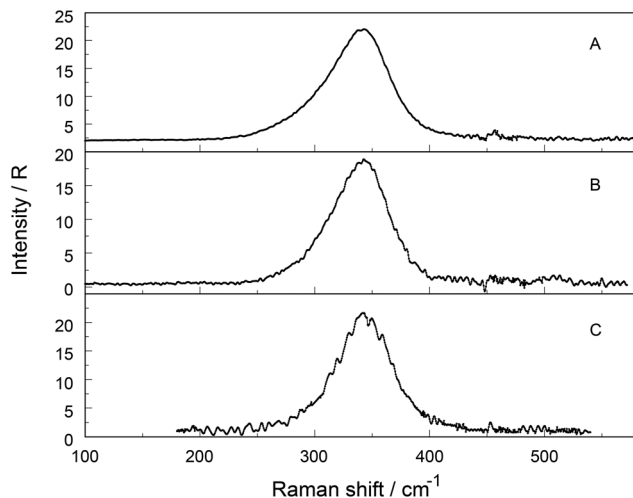


Fig. 3 Baseline corrected isotropic Raman scattering profiles of $\text{La}(\text{ClO}_4)_3(\text{aq})$. (A) 2.488 mol L^{-1} with $R_w = 15.7$; (B) 1.244 mol L^{-1} with $R_w = 37.24$ and (C) 0.249 mol L^{-1} with $R_w = 213.75$.

tioned above and the broadening of the $\nu_1 \text{LaO}_9$ band. In a $0.248 \text{ mol L}^{-1} \text{La}(\text{ClO}_4)_3$ solution, however, the νLaO_9 mode appears at 343 cm^{-1} as a much narrower band with a full width at half height (fwhh) at $\sim 49 \text{ cm}^{-1}$ and the slight contribution at 308 cm^{-1} has almost vanished. Furthermore, to rule out a hydrolysis effect, ternary solutions $\text{La}(\text{ClO}_4)_3/\text{HClO}_4/\text{H}_2\text{O}$ were studied. $\text{La}(\text{ClO}_4)_3$ solution at 2.160 mol L^{-1} plus $1.518 \text{ mol L}^{-1} \text{HClO}_4$ and a more dilute one at $1.080 \text{ mol L}^{-1} \text{La}(\text{ClO}_4)_3$ plus $0.759 \text{ mol L}^{-1} \text{HClO}_4$ were measured in the terahertz frequency range in order to check for the influence of the hydrolysis of $\text{La}^{3+}(\text{aq})$. Isotropic bands at 341 and 343 cm^{-1} respectively appear which showed 15% larger fwhh than the bands in $\text{La}(\text{ClO}_4)_3(\text{aq})$ without additional HClO_4 . This result shows that the hydrolysis of La^{3+} cannot be the reason for the variation of the band parameters such as peak position and fwhh of the isotropic La–O mode with concentration and reinforces the assumption of contact-ion-pair formation in the most concentrated solutions.

Perchlorate as an oxy-poly-anion possesses internal modes in addition to the nona-aqua La^{3+} ion. The perchlorate modes are well characterized and only a brief description shall be given.^{24,25,44} The ClO_4^- ion possesses T_d symmetry and has nine modes of internal vibrations spanning the representation $\Gamma_{\text{vib}}(T_d) = a_1(\text{Ra}) + e(\text{Ra}) + 2f_2(\text{Ra}, \text{i.r.})$. All n.m. are Raman active, but in i.r. only the f_2 modes are active. The spectra of $\text{La}(\text{ClO}_4)_3(\text{aq})$ show the predicted four Raman-active bands for the tetrahedral $\text{ClO}_4^-(\text{aq})$. The $\nu_1(a_1) \text{ClO}_4^-$ band centred at 931.5 cm^{-1} is totally polarized ($\rho = 0.005$) whereas $\nu_3(f_2) \text{ClO}_4^-$ centred at 1105 cm^{-1} is depolarized as are the deformation modes $\nu_4(f_2) \text{ClO}_4^-$ at 631 cm^{-1} and $\nu_2(e) \text{ClO}_4^-$ at 463 cm^{-1} (see Fig. 2). The $\nu_1(a_1) \text{ClO}_4^-$ band in a $\text{La}(\text{ClO}_4)_3$ solution at 2.488 mol L^{-1} appears at 934.5 cm^{-1} three wavenumbers higher than the peak position of $\text{ClO}_4^-(\text{aq})$ in very dilute solution (931.5 cm^{-1}) and as a much broader band (fwhh = 13 cm^{-1}) compared with the fwhh = 7.2 cm^{-1} for dilute

$\text{NaClO}_4(\text{aq})$ indicating, therefore, two different sites for the ClO_4^- ion.

The effect of deuteration on the LaO_9 mode of $[\text{La}(\text{OD}_2)_9]^{3+}$ was studied in $\text{La}(\text{ClO}_4)_3\text{-D}_2\text{O}$ solution and resulted in a shift of the La–O mode down to 312 cm^{-1} . The shift of ν_1 on deuteration is given by $\nu'_1 = \nu_1[m(\text{H}_2\text{O})/m(\text{D}_2\text{O})]^{1/2} = 343.5\sqrt{(18.02/20.03)} = 309 \text{ cm}^{-1}$. (As previously mentioned, water respectively heavy water molecules are viewed as point masses.)

In addition to the isotropic mode, $\nu_1 \text{LaO}_9$ of $[\text{La}(\text{OH}_2)_9]^{3+}$ at 343 cm^{-1} (fwhh = $49 \pm 2 \text{ cm}^{-1}$) a very weak, broad mode centered at $160 \pm 10 \text{ cm}^{-1}$ can be observed in aqueous $\text{La}(\text{ClO}_4)_3$ solution (isotropic Raman scattering). This mode can also be seen in pure water at $\sim 175 \text{ cm}^{-1}$ and is moderately intense but slightly polarized. This mode has been assigned to a restricted translational mode of the H-bonded water molecules. The mode is strongly anion and concentration dependent.^{32,45} It should be pointed out that in concentrated $\text{La}(\text{ClO}_4)_3$ solutions other H-bonds are important, namely $\text{OH}\cdots\text{ClO}_4^-$ and the intensity of the band due to $\text{OH}\cdots\text{ClO}_4^-$ is weak in the isotropic Raman spectrum. The strengths of the $\text{OH}\cdots\text{OClO}_3^-$ is weaker than the $\text{O}\cdots\text{OH}$ bonds in bulk water, and therefore the frequency of this mode is shifted slightly to lower frequencies compared to the restricted translation mode of neat water.^{24,25}

Relative intensity measurements confirm that the scattering intensity of $\nu_1 \text{La-O}$ mode is very weak and this may be the reason why the mode was observed as an obscured shoulder in aqueous La^{3+} salt solutions in previous publications.^{21,22} The scattering coefficient, S_h for the $\nu_1 \text{La-O}$ mode at 0.025 is very small. The S_h values, defined as the R-corrected relative scattering efficiency of the $\text{M}(\text{III})\text{-O}$ bands, were published for a variety of stretching modes of hexa-aqua metal ions, ν_1 of $[\text{M}(\text{III})(\text{OH}_2)_6]^{3+}$ in solution^{24–27,46} ($\text{M}(\text{III})$ denotes different trivalent metal cations, such as Al^{3+} , Ga^{3+} , In^{3+} etc.) The S_h value for the La–O symmetric stretching mode is smaller than the value for the $\nu_1 \text{Al-O}$ mode of $[\text{Al}(\text{H}_2\text{O})_6]^{3+}$ ($S_h(\nu_1 \text{AlO}_6) = 0.033$)^{46,47} but considerably smaller compared to other scattering intensities of group III metal cation hexa-hydrates. For the ν_1 modes for $[\text{Ga}(\text{H}_2\text{O})_6]^{3+}$ (ref. 24) and $[\text{In}(\text{H}_2\text{O})_6]^{3+}$ (ref. 25) relative intensities were measured at 0.14 and 0.22 respectively which are one order of magnitude larger than the value for $\nu_1 \text{LaO}_9$ of $[\text{La}(\text{OH}_2)_9]^{2+}$. The very small molar scattering values for La^{3+} compared to those of the higher group III metal cations such as Ga^{3+} and In^{3+} reflects the low polarizability of the former and the higher polarizability of the latter. La^{3+} is a hard cation, reflected by its scattering intensity and according to the HSAB concept of Pearson⁴⁸ and is indeed classified as such.

In $\text{La}(\text{CF}_3\text{SO}_3)_3(\text{aq})$ the La–O band is almost completely overlapped with a triflate band at 320.5 cm^{-1} but a slight asymmetry at 343 cm^{-1} reveals a second band contribution. A band separation procedure resulted in two component bands. The first band at 320.5 cm^{-1} with a very high intensity was assigned to a triflate-band and the second much weaker contribution at 343 cm^{-1} (fwhh = 49 cm^{-1}) assigned as the symmetric La–O stretching mode of $[\text{La}(\text{H}_2\text{O})_9]^{3+}$.

The DFT frequency of the ν_1 LaO₉ for [La(H₂O)₉]³⁺ imbedded in a polarizable dielectric continuum accounting for the bulk water phase was calculated at 328.2 cm⁻¹ in satisfactory agreement with the measured value. The ν_1 LaO₉ mode of the gas phase cluster of [La(H₂O)₉]³⁺ at 297.4 cm⁻¹ appears at a much lower frequency compared with the measured value. This fact is due to the lack of a second hydration sphere, discussed in greater detail in previous works.⁴⁶ All the frequencies for the [La(H₂O)₉]³⁺ species with its 78 n.m. (imbedded in a polarizable dielectric continuum) are given in Table S2 of the ESI.† The frequencies were calculated with a mixed basis set LANL2DZ/6-31G.

Results of the comparative *ab initio* molecular orbital calculations and DFT investigations (see Table S1†), demonstrate the influence of the polarizable dielectric continuum on [La(OH₂)₉]³⁺ as well as the application of polarization functions on the geometry and the symmetric La–O stretching frequency. Adding polarization functions, however, resulted in two imaginary frequencies applying PCM (Table S1†). It should be stressed that the effect of using different methods/basis sets (provided that they are at a high level) does not lead to a large effect on La–O bond length and frequency of ν_1 LaO₉ but the application of a polarizable continuum shows a much more pronounced effect (see results of Table S1† and discussions below).

To summarize, the strongly polarized, weak and broad band in the Raman spectra of dilute La(ClO₄)₃(aq) and La(CF₃SO₃)₃(aq) at 343 cm⁻¹ (fwhh = 49 cm⁻¹) is due to symmetric stretching band of the LaO₉ skeleton. The slight down shift and broadening of the ν_1 LaO₉ mode and the appearance of an asymmetry at 308 cm⁻¹ at La(ClO₄)₃(aq) concentrations >1 mol L⁻¹ indicated the existence of ion pairs formed between La³⁺ and ClO₄⁻. The perchlorate-band, ν_1 ClO₄⁻ at 934.5 cm⁻¹ and the deformation modes are much broader than in dilute solution supporting the existence of ion-pairs in these concentrated solutions.

3.3. LaCl₃(aq)

A 3.05 mol L⁻¹ LaCl₃ solution ($R_w = 16.07$) is presented in Fig. 4 in the wavenumber range from 75–700 cm⁻¹ in R-format. The La–O stretching mode in this solution is down shifted and appears at 326 cm⁻¹ and an isotropic component at 205 cm⁻¹ is observed. This finding is clear evidence that Cl⁻ has penetrated into the first hydration shell of La³⁺. The second isotropic component at 205 cm⁻¹ may be assigned to a La–Cl stretching mode of the La³⁺-chloro-complex of the form [La(OH₂)_{9-n}Cl_n]⁺³⁻ⁿ with $n = 1$ and 2. With dilution, the La–O mode shifts to higher wavenumbers. For a 2.03 mol L⁻¹ LaCl₃ solution (solute to water ratio 1 to 25.2) the band appears at 338 cm⁻¹, at a concentration at 1.013 mol L⁻¹ ($R_w = 52.5$) the La–O mode appears at 340 cm⁻¹ and for a solution at 0.501 mol L⁻¹ the mode appears at 342 cm⁻¹. This fact shows that with dilution of these concentrated solutions, the chloro-complex formation disappears and extrapolation of our Raman data leads to the conclusion that in LaCl₃(aq) < 0.2 mol L⁻¹ La³⁺ is fully hydrated. To verify, chloro-complex formation in

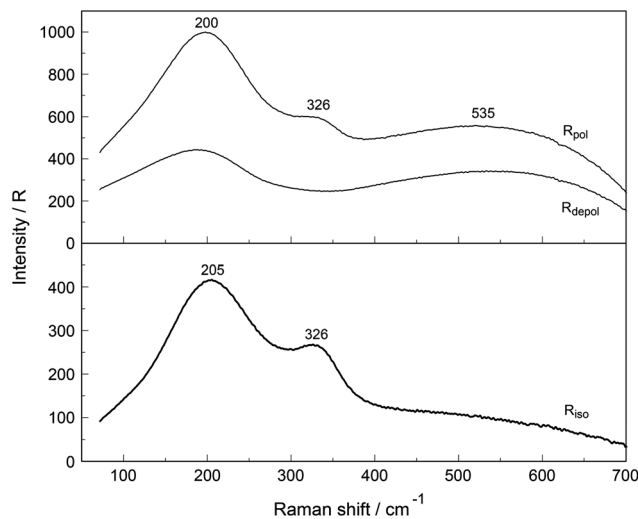
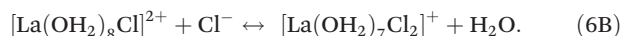


Fig. 4 Raman scattering spectra in R-format of a 3.05 mol L⁻¹ LaCl₃ solution. Upper panel: Polarized and depolarized scattering profiles. Lower panel: isotropic scattering. Note the large downshift of the La–O mode at 326 cm⁻¹ compared to the one in La(ClO₄)₃(aq) (compare with Fig. 2 and 3) is due to the penetration of Cl⁻ into the first hydration sphere and forming [La(OH₂)_{9-n}Cl_n]⁺³⁻ⁿ. Note the extremely broad mode at 535 cm⁻¹ which is due to the librational water band influenced by the solute. The mode at 205 cm⁻¹ is due to the restricted O–H...O band of H₂O and the broad feature at ~240 cm⁻¹ is assigned to ν La³⁺–Cl⁻.

LaCl₃(aq) solutions with additional HCl were investigated. A concentration profile of isotropic spectra of LaCl₃–HCl solutions at a fixed concentration of LaCl₃ at 2.03 mol L⁻¹ with 0.0, 1.0 and 4.0 mol L⁻¹ HCl added is shown in Fig. 5. The isotropic band at 339 cm⁻¹ for LaCl₃ without added HCl shifts to 336 cm⁻¹ with 1.0 mol L⁻¹ HCl added and to 326 cm⁻¹ with 4.0 mol L⁻¹ additional HCl. Fig. 6 presents a difference spectrum of LaCl₃(aq) at 2.03 mol L⁻¹ plus 4.0 mol L⁻¹ HCl(aq) from which the isotropic scattering profile of a 4 mol L⁻¹ was subtracted and a broad band at 329 cm⁻¹ is revealed, a broad band at 228 cm⁻¹ and in addition a smaller scattering contribution at 102 cm⁻¹. Clearly, the formation of the chloro-complex increases with an increase in Cl⁻ concentration according to eqn (6A):



and with an increase in Cl⁻ a second chloro-complex may be formed according to eqn (6B):



The estimated value of the log β_1 value for eqn (6A) equal to ~0.1 reveals the weak nature of the chloro-complex in LaCl₃(aq) at 23 °C. Thermodynamic data on the chloro-complex formation in LaCl₃(aq) confirm this weak nature of the complexes and equilibrium constants for reaction 6A and B may be found in ref. 49 and 50. The existence of a weak chloro-complex species in LaCl₃(aq) using Raman spectroscopy in the terahertz region of the scattering spectra was presented recently using Raman spectroscopy.²³ In the most concen-

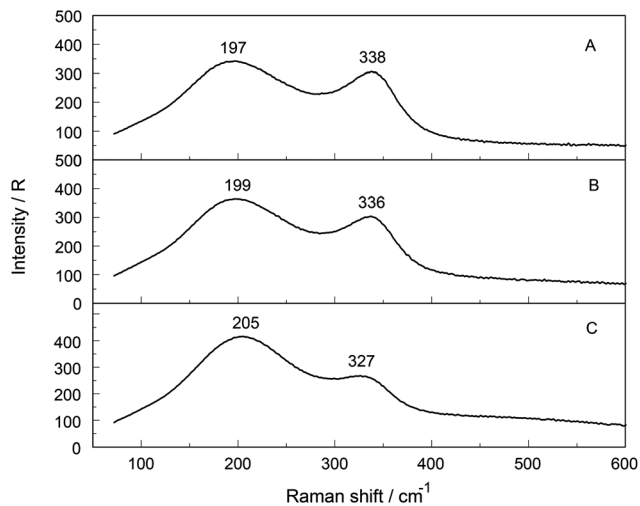


Fig. 5 Isotropic Raman spectra of a 2.03 mol L⁻¹ LaCl₃ solution and two solutions with additionally HCl added. (A) 2.03 mol L⁻¹ LaCl₃ without HCl added; (B) 2.03 mol L⁻¹ LaCl₃ + 1 mol L⁻¹ HCl and (C) 2.03 mol L⁻¹ LaCl₃ + 4 mol L⁻¹ HCl.

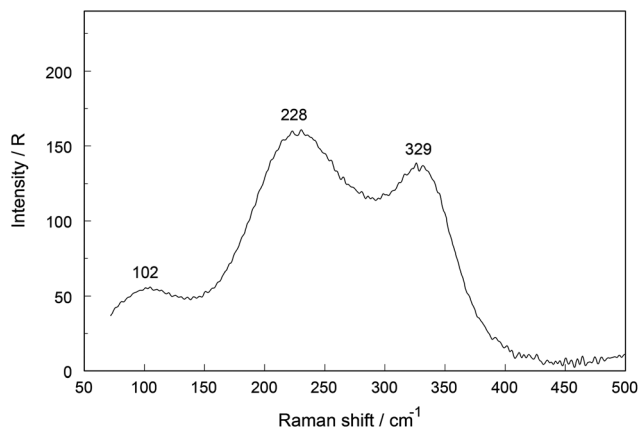


Fig. 6 Difference Raman spectra of the isotropic scattering profile of 2.03 mol L⁻¹ LaCl₃(aq) from which a isotropic profile of HCl(aq) at 4.0 mol L⁻¹ was subtracted. The band at 329 cm⁻¹ stems from the La–O mode of the complex, [La(OH₂)_{9-n}Cl_n]⁺³⁻ⁿ, and the broad mode at 228 cm⁻¹ from the La–Cl vibrations of the complex.

trated LaCl₃ solution, the mole ratio solute to water is 1 to 16.1 which means that there are not enough water molecules to form a second hydration sphere around all ions forcing outer-shell ion pairs. The chloride ions penetrate the flexible hydration shell of La³⁺ into the first hydration shell. In concentrated AlCl₃ solutions, however, Cl⁻ does not penetrate into the first hydration shell of Al³⁺.^{46,47} The hydration shell of [Al(OH₂)₆]³⁺ is quite inert. Further experimental support for Cl⁻ penetrating into the first hydration shell of La³⁺ and formation of chloro-complex formation comes from a recent combined neutron scattering and X-ray scattering study in which information was incorporated from Extended X-ray Absorption Fine Structure (EXAFS) spectroscopy data¹⁵ into their applied analytical data treatment. This high quality structural study¹⁵

on a 1.0 mol kg⁻¹ LaCl₃(aq) showed that La³⁺ is hydrated by eight water molecules and one chloride ion, forming an inner-sphere ion complex in which the water molecules maintain angular configurations consistent with a tricapped trigonal prism configuration. In an earlier EXAFS study on LaCl₃(aq) and LaCl₃(aq) plus an excess of LiCl, it was also demonstrated that Cl⁻ forms chloro-complexes in concentrated LaCl₃ solutions.¹¹

To summarize, the [La(OH₂)_{9-n}Cl_n]⁺³⁻ⁿ modes in chloride solutions could be detected and formation of weak chloro-complexes with La³⁺ were verified. In dilute solutions (*c* < 0.05 mol L⁻¹) the chloro-complex species disappeared upon dilution and [La(OH₂)₉]³⁺ and Cl⁻(aq) are formed. The chloro-complex formation may be one reason for the data scatter in the La–O bond distance and coordination numbers presented for La³⁺(aq). This fact was also pointed out in a recent experimental structural study.¹⁵

3.4. La(NO₃)₃(aq)

When nitrate replaces water in the first coordination sphere of a cation, marked changes occur in the spectrum of the ligated nitrate, so that it is possible to differentiate between the modes of the ligated and the unligated nitrate. Nitrate-complex formation was observed for a variety of divalent and trivalent metals in solutions.^{24,25,46} The modes of the unligated nitrate, the fully hydrated nitrate, NO₃⁻(aq), were measured recently^{24–26,46} and the Raman spectrum for a 0.409 mol L⁻¹ NaNO₃(aq) (*R_w* = 134.07) is given in Fig. S2† together with the vibrational spectroscopic data of the bands and their assignment in Table S3, ESI.† Nitrate-complex formation is not only characterized by the ligated NO₃⁻ but also by the fact that the Mⁿ⁺–O symmetric stretch of the metal ions (Mⁿ⁺ = metal ion) split into a band of the fully hydrated cation and a band of the partially hydrated metal ion as well as a ligand mode Mⁿ⁺–Lⁿ⁻ (L = NO₃⁻).

A brief summary for the vibrational data on NO₃⁻(aq) shall be presented before discussing the spectroscopic features in La(NO₃)₃(aq). The “free” NO₃⁻ anion possesses D_{3h} symmetry and four modes should be observed (two doubly degenerate). The n.m. span the representation $\Gamma_{\text{vib}}(D_{3h}) = a'_1(\text{Ra}) + a'_2(\text{i.r.}) + 2e'(\text{Ra}, \text{i.r.})$. The $\nu_1(a'_1)$ symmetric N–O stretching mode is Raman active but forbidden in infrared, while the *e'* modes, ν_3 (antisymmetric N–O stretch) and ν_4 (in-plane bending mode) are Raman and infrared active. The out-of plane deformation mode with the character a''_2 is only infrared active. In NO₃⁻(aq), the polarized Raman mode at 1047.4 cm⁻¹ is the strongest band in Raman scattering and appears quite narrow with a fwhh = 6.55 cm⁻¹. This band is assigned to the symmetric N–O stretch vibration, $\nu_1(a'_1)$. Its depolarization degree at 0.034 is quite low and confirms that it represents a symmetrical n.m. The mode $\nu_3(e')$, the asymmetric N–O stretching mode which is depolarized and relatively weak, appears not as a single band but shows two band components at 1347 and 1409 cm⁻¹. The band contour appears as a doublet even in very dilute solutions of NaNO₃(aq). Asymmetric hydration of the nitrate anion in aqueous solution is the reason for this

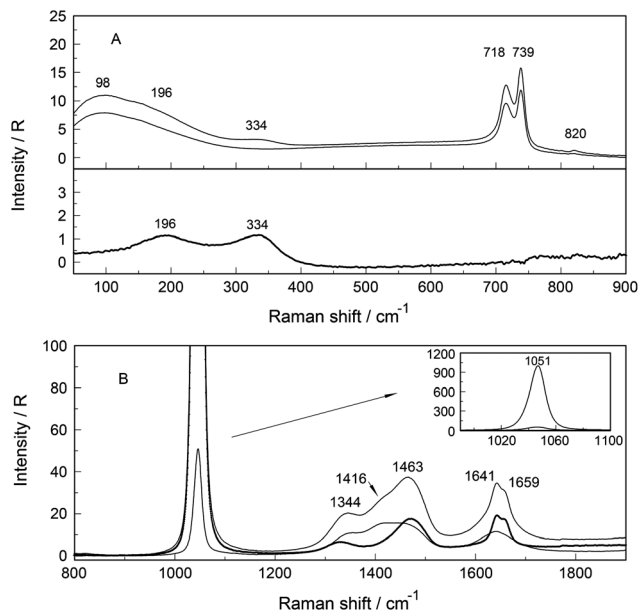


Fig. 7 Raman spectrum of a 1.844 mol L⁻¹ La(NO₃)₃ solution from 45–1900 cm⁻¹. Panel A: Low wavenumber region (45–900 cm⁻¹). The upper part of panel A shows the R_{pol} and R_{depol} scattering while R_{iso} is underneath. Panel B: Higher wavenumber region (from 800–1900 cm⁻¹); the isotropic scattering contribution is given in bold. The inset depicts the NO₃⁻(aq) mode at 1051 cm⁻¹ at its full intensity scale.

double band (*cf.* for instance ref. 24, 25 and 51). The depolarized mode $\nu_4(e')$ at 718 cm⁻¹ is active in Raman and infrared and is much weaker than the symmetric stretching mode $\nu_1(a'_1)$. The infrared active mode, $\nu_2(a''_2)$ occurs at 828 cm⁻¹ and its overtone $2 \times \nu_2$ at 1658 cm⁻¹ is Raman active (a'_1) and appears polarized.

An overview Raman spectrum of a 1.844 mol L⁻¹ La(NO₃)₃ solution in R-format from 45–1900 cm⁻¹ is presented in Fig. 7 and more detailed spectrum in the $\nu_3(e')$ antisymmetric stretching region and $2 \nu_2$ overtone region is presented in Fig. S3.† A concentration series of polarized Raman spectra in R-format of four La(NO₃)₃ solutions at 1.844 mol L⁻¹ ($R_w = 26.09$), 1.050 mol L⁻¹ ($R_w = 49.10$), 0.466 mol L⁻¹ ($R_w = 115.26$) and 0.121 mol L⁻¹ ($R_w = 455.3$) from 150 to 1800 cm⁻¹ wavenumbers are presented in Fig. 8 and in more detail the $\nu_1(a'_1)$ bands in Fig. S4.† The nitrate bands split into bands of unligated (free), hydrated nitrate, NO₃⁻_{free} and nitrate bound, NO₃⁻_{bound} to La³⁺. The Raman spectra of La(NO₃)₃(aq) are more complex than the ones for NaNO₃(aq) and it is immediately clear that the nitrate penetrated into the first hydration sphere of La³⁺. The splitting of the $\nu_3(e')$ bending mode into bands at 717 and 739 cm⁻¹ in La(NO₃)₃(aq), the asymmetry and broadening of the ν_1 band of NO₃⁻ which appears at slightly higher wavenumbers, at 1051 cm⁻¹ and the broadening and additional splitting of the $\nu_3(e')$ band (additional isotropic band contributions at 1328, and 1470 cm⁻¹ appear in La(NO₃)₃(aq)) are clear indications that NO₃⁻ penetrated into the first hydration sphere of La³⁺. Furthermore, the Raman

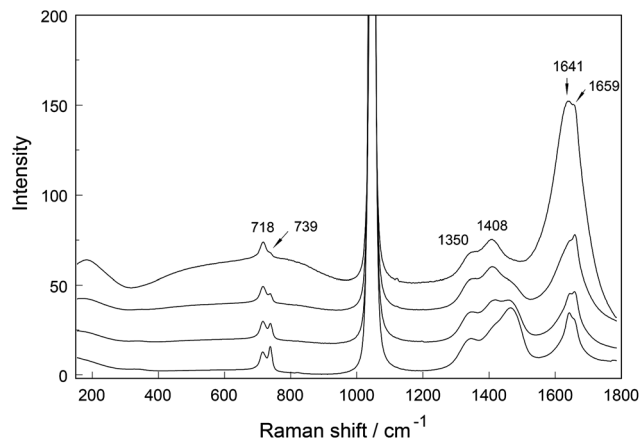
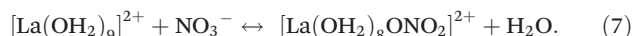


Fig. 8 Raman spectra (R-polarized) of four La(NO₃)₃ solutions; from bottom to top: 1.844, 1.050, 0.466 and 0.121 mol L⁻¹ in solute concentration. Note that the ν_1 N–O stretching mode at ~ 1047 cm⁻¹, at its full scale, is given in Fig. S3† for more detail. The bands between 1200 and 1800 cm⁻¹ are given in more detail in Fig. S3–S5.†

inactive mode, $\nu_2(a''_2)$ appears as a very weak but broad band contour in the Raman spectrum in La(NO₃)₃(aq) at 1.844 mol L⁻¹ at ~ 822 cm⁻¹ and its Raman active overtone, $2\nu_2(a'_1)$ appears as two bands at 1642 and 1656 cm⁻¹ (Fig. 7, lower panel).

In the aqueous La(NO₃)₃ solutions at 1.844 mol L⁻¹, the weak symmetric stretching mode of the La–O at 343 cm⁻¹ is even broader and shifts to 334 cm⁻¹ (one component at 314 cm⁻¹ and a second at 343 cm⁻¹). The ligand mode of the nitrate-complex appears as a polarized band at 196 cm⁻¹. For quantitative purposes, the broad ν_1 La–O band was fitted with two Gauss-Lorentz band components. The first component at 343 cm⁻¹ (fwhh = 49 cm⁻¹) is indicative of the nona-aqua-La³⁺ species, [La(OH₂)₉]³⁺, while the second band component at ~ 314 cm⁻¹ (fwhh ~ 52 cm⁻¹) is due to the hydrated lanthanum-nitrato complex, [La(OH₂)_{9-n}(NO₃)_n]³⁻ⁿ. The quantitative data of the band fits are given in Table S4.†

In the concentrated solution 44% of the La³⁺ exist as a nitrato complex while in the dilute solution at 0.121 mol L⁻¹ the La³⁺ exist only to 12% in form of a nitrato complex (results in Table S3, ESI†). Upon further dilution, the nitrato-complex disappears and from extrapolations of α -values (the degree of nitrato-complex formation) as a function of solution concentration, it becomes clear that in solutions < 0.01 mol L⁻¹ 99% of the La³⁺ is fully hydrated and the nitrato-complex at 1% becomes insignificant. The formation of the nitrato complex with La³⁺ may be expressed by eqn (7):



An estimate of the $\log \beta_1$ value at ~ 0.12 reveals the weak nature of the nitrato-complex in La(NO₃)₃(aq) at 23 °C. Thermodynamic data on the weak nitrato-complex formation may be found in ref. 49 and 50. Furthermore, a ¹³⁹La- and ¹H-NMR study confirmed the formation of La³⁺-nitrato complexes in mixed aqueous solutions of La(NO₃)₃(aq).⁵²

The following spectroscopic features of the ligated NO_3^- are evident for the formation of a nitrate-complex: In the bending mode region a band component of the bending mode, $\nu_4(e')$ NO_3^- appears at 739 cm^{-1} in $\text{La}(\text{NO}_3)_3(\text{aq})$ (see Fig. 7 and 8). A broad and asymmetric feature at 1035 cm^{-1} appears in addition to the symmetrical stretching mode of nitrate, the $\nu_1(a_1')$ NO_3^- which appears at 1051 cm^{-1} . The doublet structure assigned to the antisymmetric stretch of N–O, $\nu_3(e')$ NO_3^- which appears in free NO_3^- at 1348 and 1407 cm^{-1} shows several bands in the polarized and depolarized scattering (see Fig. 7 and 8) and in addition two broad bands at 1330 and 1470 cm^{-1} in the isotropic scattering. These bands are most pronounced in concentrated $\text{La}(\text{NO}_3)_3(\text{aq})$ and diminish with dilution. The overtone, $2\nu_2$ of the infrared active mode ν_2 splits into two narrow bands namely at 1659 cm^{-1} (free NO_3^-) and a band at 1641 cm^{-1} (bound NO_3^-). Again, with dilution the band at 1641 cm^{-1} vanishes and the one for free NO_3^- at 1660 cm^{-1} is still observable. This is demonstrated in Fig. S5, ESI,† where the isotropic profiles of four $\text{La}(\text{NO}_3)_3$ solutions are shown in the wavenumber range from 1200 – 1800 cm^{-1} (bands of $\nu_3(e')$ NO_3^- and $2\nu_2$). Furthermore, the ligand mode of the nitrate-complex, $\text{La}^{3+}\text{-ONO}_2^-$ appears at 196 cm^{-1} . The situation in concentrated $\text{La}(\text{NO}_3)_3$ solutions is comparable to the situation in $\text{Ga}(\text{NO}_3)_3$ ²⁴ and $\text{In}(\text{NO}_3)_3$ solutions,²⁵ where nitrate complex formation is also apparent.

4. Conclusions

Raman spectra of aqueous $\text{La}(\text{III})$ -perchlorate, triflate, chloride and nitrate solutions were measured over a broad concentration range. The weak, polarized mode at 343 cm^{-1} (fwhh = 50 cm^{-1}) was assigned to ν_1 La–O of the LaO_9 skeleton. In deuterated $\text{La}(\text{ClO}_4)_3$ solution, a mode at 312 cm^{-1} was assigned to ν La–O of the $[\text{La}(\text{OD}_2)_9]^{3+}$. The Raman spectroscopic data suggest that the $[\text{La}(\text{OH}_2)_9]^{3+}$ ion is thermodynamically stable in dilute perchlorate and triflate solutions. No inner-sphere complexes in these solutions could be detected spectroscopically. Outer-sphere ion pairs of the type $\text{La}(\text{OH}_2)_9^{3+}\cdot\text{ClO}_4^-$ are formed in concentrated $\text{La}(\text{ClO}_4)_3(\text{aq})$. DFT frequency calculations of a $[\text{La}(\text{OH}_2)_9]^{3+}$ imbedded in a polarizable dielectric continuum gave a ν_1 La–O equal to 328 cm^{-1} in fair agreement with the experiment. The bond distances and angles of the $[\text{La}(\text{OH}_2)_9]^{3+}$ embedded in a polarizable dielectric continuum were also presented. The symmetry of the aqua complex is D_3 .

In LaCl_3 solutions Cl^- penetrates the first hydration sphere of $\text{La}^{3+}(\text{aq})$ and chloro-complexes are formed. However, the chloro complexes disappear rapidly upon dilution and at a concentration $<0.05\text{ mol L}^{-1}$ the chloro complexes have almost disappeared. This Raman spectroscopic finding was substantiated applying neutron – and X-ray scattering as well as EXAFS.^{11,15}

In $\text{La}(\text{NO}_3)_3$ solutions NO_3^- penetrates the first hydration sphere of La^{3+} and the nitrate complex was characterized;

the nitrate complex disappears fairly rapidly upon dilution; $<0.05\text{ mol L}^{-1}$ the nitrate-complexes have disappeared.

Acknowledgements

WWR and GI wish to thank Frau B. Ostermay for her skilful technical assistance.

Notes and references

- 1 *The Rare Earth Elements: Fundamentals and Applications*, ed. D. A. Atwood, J. Wiley & Sons Ltd., 2012.
- 2 A. He, F. Zhou, F. Ye, Y. Zhang, X. He, X. Zhang, R. Guo, X. Zhao, Y. Sun, M. Huang, Q. Li, Z. Yang, Y. Xu and J. Wu, *J. Spectrosc.*, 2013, **2013**, 593636.
- 3 A. J. Anderson, S. Jayanetti, R. A. Mayanovic, W. A. Bassett and I.-M. Chou, *Am. Mineral.*, 2002, **87**, 262–268.
- 4 A. Habenschuss and F. H. Spedding, *J. Chem. Phys.*, 1979, **70**, 3758–3763.
- 5 G. Johansson and H. Wakita, *Inorg. Chem.*, 1985, **24**, 3047–3052.
- 6 L. S. Smith and D. L. Wertz, *J. Am. Chem. Soc.*, 1975, **97**, 2365–2368.
- 7 L. S. Smith and D. L. Wertz, *J. Inorg. Nucl. Chem.*, 1977, **39**, 95–98.
- 8 M. Alves Marques, M. I. Cabaço, M. I. de Barros Marques, A. M. Gaspar and C. M. de Morais, *J. Phys.: Condens. Matter*, 2001, **13**, 4367–4386.
- 9 J. A. Solera, J. García and M. G. Proietti, *Phys. Rev. B: Condens. Matter*, 1995, **51**, 2678–2686.
- 10 S. Ishiguro, Y. Umabayashi and M. Komiyama, *Coord. Chem. Rev.*, 2002, **226**, 103–111.
- 11 P. G. Allen, J. J. Bucher, D. K. Shuh, N. M. Edelstein and I. Craig, *Inorg. Chem.*, 2000, **39**, 595–601.
- 12 J. Näslund, P. Lindqvist-Reis, I. Persson and M. Sandström, *Inorg. Chem.*, 2000, **39**, 4006–4011.
- 13 P. D'Angelo, S. De Panfilis, A. Filippini and I. Persson, *Chem. – Eur. J.*, 2008, **14**, 3045–3055.
- 14 I. Persson, P. D'Angelo, S. De Panfilis, M. Sandström and L. Eriksson, *Chem. – Eur. J.*, 2008, **14**, 3056–3066.
- 15 S. Díaz-Moreno, S. Ramos and D. T. Bowron, *J. Phys. Chem. A*, 2011, **115**(24), 6575–6581.
- 16 K. Djanashvili, C. Platas-Iglesia and J. A. Peters, *Dalton Trans.*, 2008, 602–607.
- 17 C. Clavaguera, R. Pollet, J. M. Soudan, V. Brenner and J. P. Dognon, *J. Phys. Chem. B*, 2005, **109**, 7614–7616.
- 18 M. Duvail, R. Spezia, M. Souaille, T. Cartailier and P. Vitorge, *J. Chem. Phys.*, 2007, **127**, 034503.
- 19 M. Duvail, P. Vitorge and R. Spezia, *J. Chem. Phys.*, 2009, **130**, 104501–104513.
- 20 O. M. D. Lutz, T. S. Hofer, B. R. Randolph and B. M. Rode, *Chem. Phys. Lett.*, 2012, **536**, 50–54.
- 21 H. Kanno, *J. Alloys Compd.*, 1993, **192**, 271–273.
- 22 H. Kanno, *J. Phys. Chem.*, 1988, **92**, 4232–4236.

- 23 W. W. Rudolph, D. Fischer, G. Irmer and C. C. Pye, *Proceedings of the XXI International Conference on Raman Spectroscopy*, ed. R. Whithnall and B. Z. Chowdhry, IM Publications, Charlton, Chichester, 2008, pp. 672–673.
- 24 W. W. Rudolph and G. Irmer, *Dalton Trans.*, 2013, 3919–3935.
- 25 W. W. Rudolph and G. Irmer, *Dalton Trans.*, 2013, 14460–14472.
- 26 W. W. Rudolph and C. C. Pye, *Phys. Chem. Chem. Phys.*, 2002, **4**, 4319–4327.
- 27 W. W. Rudolph, D. Fischer, M. R. Tomney and C. C. Pye, *Phys. Chem. Chem. Phys.*, 2004, **6**, 5145–5155.
- 28 W. W. Rudolph and G. Irmer, *Appl. Spectrosc.*, 2007, **61**, 1312–1327.
- 29 A. I. Vogel, *A Text-Book of Quantitative Inorganic Analysis*, Longman, London, 3rd edn, 1961.
- 30 F. H. Spedding, M. J. Pikal and B. O. Ayers, *J. Phys. Chem.*, 1966, **70**, 2440–2449; see p. 2441.
- 31 W. W. Rudolph, D. Fischer and G. Irmer, *Appl. Spectrosc.*, 2006, **60**, 130.
- 32 W. W. Rudolph, M. H. Brooker and C. C. Pye, *J. Phys. Chem.*, 1995, **99**, 3793.
- 33 M. J. Frisch, G. W. Trucks, H. B. Schlegel, G. E. Scuseria, M. A. Robb, J. R. Cheeseman, J. A. Montgomery Jr., T. Vreven, K. N. Kudin, J. C. Burant, J. M. Millam, S. S. Iyengar, J. Tomasi, V. Barone, B. Mennucci, M. Cossi, G. Scalmani, N. Rega, G. A. Petersson, H. Nakatsuji, M. Hada, M. Ehara, K. Toyota, R. Fukuda, J. Hasegawa, M. Ishida, T. Nakajima, Y. Honda, O. Kitao, H. Nakai, M. Klene, X. Li, J. E. Knox, H. P. Hratchian, J. B. Cross, V. Bakken, C. Adamo, J. Jaramillo, R. Gomperts, R. E. Stratmann, O. Yazyev, A. J. Austin, R. Cammi, C. Pomelli, J. W. Ochterski, P. Y. Ayala, K. Morokuma, G. A. Voth, P. Salvador, J. J. Dannenberg, V. G. Zakrzewski, S. Dapprich, A. D. Daniels, M. C. Strain, O. Farkas, D. K. Malick, A. D. Rabuck, K. Raghavachari, J. B. Foresman, J. V. Ortiz, Q. Cui, A. G. Baboul, S. Clifford, J. Cioslowski, B. B. Stefanov, G. Liu, A. Liashenko, P. Piskorz, I. Komaromi, R. L. Martin, D. J. Fox, T. Keith, M. A. Al-Laham, C. Y. Peng, A. Nanayakkara, M. Challacombe, P. M. W. Gill, B. Johnson, W. Chen, M. W. Wong, C. Gonzalez and J. A. Pople, *GAUSSIAN 03 (Revision C.02)*, Gaussian, Inc., Wallingford, CT, 2004.
- 34 C. Lee, W. Yang and R. C. Parr, *Phys. Rev. B: Condens. Matter*, 1988, **37**, 785–789.
- 35 A. D. Becke, *J. Chem. Phys.*, 1993, **98**, 5648–5655.
- 36 M. Cossi, G. Scalmani, N. Rega and V. Barone, *J. Chem. Phys.*, 2002, **117**, 43–54.
- 37 D. P. Fay, D. Litchinsky and N. Purdie, *J. Phys. Chem.*, 1969, **73**, 544–552.
- 38 D. P. Fay and N. Purdie, *J. Phys. Chem.*, 1970, **74**, 1160–1166.
- 39 L. Helm and A. E. Merbach, *Chem. Rev.*, 2005, **105**, 1923–1959.
- 40 W. Rudolph and S. Schönherr, *Z. Phys. Chem.*, 1989, **270**, 1121–1134.
- 41 B. Auer, R. Kumar, J. R. Schmidt and J. L. Skinner, *Proc. Natl. Acad. Sci. U. S. A.*, 2007, **104**, 14215–14220.
- 42 B. M. Auer and J. L. Skinner, *J. Chem. Phys.*, 2008, **128**, 224511.
- 43 M. H. Brooker, G. Hancock, B. C. Rice and J. Shapter, *J. Raman Spectrosc.*, 1989, **20**, 683–694.
- 44 C. I. Ratcliffe and D. E. Irish, *Can. J. Chem.*, 1985, **63**, 3521–3525.
- 45 G. E. Walrafen, *J. Chem. Phys.*, 1962, **36**, 1035–1042.
- 46 W. W. Rudolph, R. Mason and C. C. Pye, *Phys. Chem. Chem. Phys.*, 2000, **2**, 5030–5040.
- 47 W. Rudolph and S. Schönherr, *Z. Phys. Chem.*, 1991, **172**, 31–48.
- 48 R. G. Pearson, *J. Am. Chem. Soc.*, 1963, **85**, 3533–3539.
- 49 S. A. Wood, *Chem. Geol.*, 1990, **82**, 159–186.
- 50 J. Schijf and R. H. Byrne, *Geochim. Cosmochim. Acta*, 2004, **68**, 2825–2837.
- 51 J. Thøgersen, J. Réhault, M. Odellius, T. Ogden, N. K. Jena, S. J. Jensen, S. R. Keiding and J. Helbing, *J. Phys. Chem. B*, 2013, **117**, 3376–3388.
- 52 A. Fratiello, V. Kubo-Anderson, T. Bolinger, C. Cordero, B. DeMerit, T. Flores and R. D. Perrigan, *J. Solution Chem.*, 1989, **18**, 313–330.